Flow Patterns in the Vicinity of Triple Line Dynamics Arising from a Local Surface Tension Model

J. Monnier and I. Cotoi

Laboratoire de Modelisation et Calcul (LMC-IMAG),
Project-Team IDOPT, BP 53, F-38041 Grenoble Cedex 9, France
{Jerome.Monnier, Cotoi}@imag.fr

Abstract. We model and simulate numerically a droplet impact onto a solid substrate. The triple line dynamics modelling is implicit (as opposed to classical explicit mobility relations), it is based on the Shikhmurzaev equations. These equations include generalized Navier slip type boundary conditions with extra local surface tension gradient terms. Numerical results when spreading and recoiling are presented. A particular attention is paid to flow patterns near the contact line.

1 Introduction

One of the main difficulty to simulate present droplet flows is the contact line dynamics modelling. This problem has been widely studied and still remains an open problem. Let us cite macroscopic models with slip boundary conditions, see [4], [5], [3], mesoscopic models with diffuse interface, see [6] and also [9], and connection with molecular dynamics, see [11]. The most frequent contact line model is an explicit mobility relation giving the contact line velocity in function of the wetting angle value at any time (Tanner type laws). Nevertheless, it has been showed, [2], that the dynamic wetting angle cannot be determined inherently by such a mobility relation.

In the present paper, we consider an "implicit" model based on the Shikhmurzaev theory, [10], [2]. This model lead to generalized Navier slip type boundary conditions with local surface tension gradient terms. It does not impose the contact line velocity nor the wetting angle since they are a response of the full model. In Section 2, we present the equations: 2D axi-symmetric Navier-Stokes equations with an ALE formulation. In Section 3, we discretize the equations using a finite element scheme. We introduce a contact line algorithm which imitates caterpillar motion observed in experiments. Curvature is computed using a local Bezier least-square approximation. In Section 4, first we consider a Tanner type law and we test the robustness of our algorithm. Then, we consider both spreading phase and recoiling phase, using the present "implicit" model based on the Shikhmurzaev theory. The extra local terms appearing in this model are setted by preliminary results presented in [7] and [8]. We show different flow patterns generated by these terms near the triple point. Finally, we obtain encouraging results for both phases.

V.N. Alexandrov et al. (Eds.): ICCS 2006, Part II, LNCS 3992, pp. 26–33, 2006.

2 Mathematical Model

2.1 Equations

The droplet dynamics is modelled by the unsteady incompressible Navier-Stokes equations 2D axi-symmetric. We denote by $\boldsymbol{u} = (u_r, u_z)^T$ the fluid velocity, p its pressure, Σ the stress tensor, D the deformation tensor and Re the Reynolds number. We denote by $(\boldsymbol{\tau}, \boldsymbol{n})$ the unit tangential and external normal vectors such that it is direct. We set: $\boldsymbol{\Sigma_n} = \Sigma.\boldsymbol{n}$; $\boldsymbol{\Sigma_n} = \Sigma_n \boldsymbol{n} + \Sigma_\tau \boldsymbol{\tau}$. The r-momentum equations with ALE formulation is:

$$Re\left(\frac{\partial u_r}{\partial t} + (\boldsymbol{u} - \boldsymbol{\gamma}) \cdot \nabla u_r\right) = -\frac{\partial p}{\partial r} + 2\left(\frac{1}{r}\frac{\partial (r\, D_{rr}(\boldsymbol{u}))}{\partial r} + \frac{\partial (D_{rz}(\boldsymbol{u}))}{\partial z} - \frac{u_r}{r^2}\right) \quad (1)$$

where $\boldsymbol{\gamma}$ is the equivalent velocity field. The z-momentum equation is similar. The continuity equation is: $\frac{1}{r}\frac{\partial (r u_r)}{\partial r} + \frac{\partial u_z}{\partial z} = 0$, with initial conditions. Boundary conditions on the free surface (liquid-gas) are:

$$\boldsymbol{\Sigma}_n \;=\; (-p_{ext} + \frac{\kappa}{Ca})\boldsymbol{n} \;+\; h\boldsymbol{\tau} \qquad \text{in } (0,T) \times \Gamma_f \quad (2)$$

where Ca is the Capillary number, κ is the mean curvature and p_{ext} is the external pressure. The extra term h is given (see Shikhmurzaev's theory below). We have classical boundary conditions on the symmetry axis. We decompose the liquid-solid interface into two parts: Γ_{ad} and Γ_{sl}. Γ_{sl} denotes a "small" part of the liquid-solid interface near the triple point. We consider a generalized Navier slip type boundary condition (local slipping):

$$\begin{cases} \boldsymbol{u}.\boldsymbol{n} &= 0 & \text{in } (0,T) \times \Gamma_{sl} \\ \Sigma_\tau &= -[\beta \boldsymbol{u} + \boldsymbol{g}].\boldsymbol{\tau} & \text{in } (0,T) \times \Gamma_{sl} \end{cases} \quad (3)$$

where β is a given sliding coefficient. The extra term $\boldsymbol{g}$ is given, it models either a surface tension gradient in the Shikhmurzaev's theory or a uncompensated Young stress in the Qian-Wang-Sheng theory, see below. On Γ_{ad}, we impose adherence boundary conditions: $\boldsymbol{u} = 0$. The free surface Γ_f is transported by $\boldsymbol{u}$, it is described by a function $\phi(t, r(t), z(t))$. We have: $\frac{d\phi}{dt} \;=\; \frac{\partial \phi}{\partial t} \;+\; \boldsymbol{u} \cdot \nabla \phi = 0$ in $(0,T) \times \Omega$, with initial conditions.

2.2 Contact Line Dynamics Modelling

We consider two different types of model for the contact line dynamics: an explicit model (Tanner type law) and an "implicit" one deriving from Shikhmurzaev theory.

Mobility relation (Tanner type Law). The contact line velocity and the wetting angle are related by:

$$U_{CL}(t) \;=\; k\, \frac{(\theta(t) - \theta^{eq})^\gamma}{(\theta^{eq})^\gamma} \quad \text{for } t \in]0,T[\quad (4)$$

where U_{CL} is the contact line velocity, θ^{eq} is the wetting angle at equilibrium (Young's law), θ is the (dynamic) wetting angle. k and γ are parameters usually determined using experimental results.

Local flow modelling and Shikhmurzaev's theory. The "implicit" model does not impose the contact line velocity and the wetting angle but consider them as a response of the model. This model is based on the Shikhmurzaev's theory, [10], [2], which makes introduce the generalized Navier slip condition (3) and the condition (2). These conditions are local since the extra terms $\boldsymbol{g}$ and h vanish except in a vicinity of the triple point. The basic idea of this theory is to consider that the rolling motion observed in experiments, [4], implies that particles of the liquid-gas interface become an element of the solid-liquid in a finite time. Then, the surface tension value associated to this particle must change to its new equilibrium value relative to the solid-liquid interface. This process would gives rise to a surface tension gradient in a small vicinity of the advancing contact line (hence a local Marangoni effect). In other respect, the Young equation would remain valid at any time. In this theory,

$$\boldsymbol{g} \;=\; -\frac{1}{2Ca}\,\boldsymbol{\nabla}\sigma \text{ and } h \;=\; \frac{1}{Ca}\,\boldsymbol{\nabla}\sigma_{LG}.\boldsymbol{\tau} \tag{5}$$

where σ and σ_{LG} are the liquid-solid and the liquid-gas surface tension coefficient respectively. In [7] and [8], a mathematical and numerical study presents some qualitative behaviors of g and h arising from Shikhmurzaev's theory.

A connection with Qian-Wang-Sheng theory. From molecular dynamics simulations on immiscible fluids, [11] shows that the relative slipping between the fluid and the solid wall follows a generalized Navier slip b.c. similar to (3) (if one phase fluid only is considered). In this theory, the extra term $\boldsymbol{g}$ in (3) would model an interfacial uncompensated Young stress. The extra tangential stress $\boldsymbol{g}$ is defined as follows: $\int_{\Gamma_{int}} g\ dy \;=\; \sigma(cos\theta - cos\theta^{eq})$, where $\int_{\Gamma_{int}}\ dy$ denotes the integral across the interface Γ_f.

3 Discretization and Algorithms

3.1 Finite Element Scheme

We discretize the full model in time using the Euler implicit scheme and a first order characteristic method. The space discretization is done using the second order Taylor-Hood finite element. The scheme is implemented using a public C++ finite element library. To compute the curvature , first we consider a second order local Bezier least-square approximation of points defining the interface, second we evaluate the curvature of the Bezier curve. We performed numerical tests which showed that this method filters noise quite reasonably while it allows to detect local and rapid variation of curvature.

3.2 The ALE Free Surface Algorithm

The free surface problem is solved using an ALE formulation and a characteristic method. The algorithm is the following. At time step n, given Ω^n and $(\boldsymbol{u}^n, p^n)$ in Ω^n.

Step 1. Compute the new free surface position Γ_f^n following the lagrangian characteristics lines (each point of the boundary is translated by $\boldsymbol{u}^n \Delta t$). Then, compute an equivalent deformation field $\boldsymbol{\gamma}^n$ preserving the mesh by solving a linear elasticity system.

Step 1bis. Compute the new solution $(\boldsymbol{u}_\tau^{n+1}, p_\tau^{n+1})$ of Navier-Stokes in Ω^n.

Step 2. Update the domain $\Omega^{n+1} = \boldsymbol{\gamma}^n(\Omega^n)$ (mesh transport by $\boldsymbol{\gamma}^n$).

Step 3. Obtain the new solution $(\boldsymbol{u}^{n+1}, p^{n+1})$ in Ω^{n+1} by setting: $\boldsymbol{u}^{n+1}|_{\Omega^{n+1}} = \boldsymbol{u}_\tau^{n+1}|_{\Omega^n}$ and $p^{n+1}|_{\Omega^{n+1}} = p_\tau^{n+1}|_{\Omega^n}$.

3.3 Spreading and Caterpillar Motion

When spreading, our algorithm imitates the caterpillar motion observed in experiments, [4]. Fig. 5 (Left) represents typical successive time steps. If at time step n, the first point (or several points) on the free surface are projected on the solid substrate, all the points on the solid wall but the last ones become no-slip points. The last two points remain slip point.

3.4 Recoiling Motion

When de-wetting (recoiling), the triple point and the slip points are allowed to move horizontally, also vertically if their vertical velocity is positive, see Fig. 5 (Right). If the triple point moves away from the solid wall, the first point to the left becomes the triple point, hence becoming a free point. The second point to the left becomes a slip point.

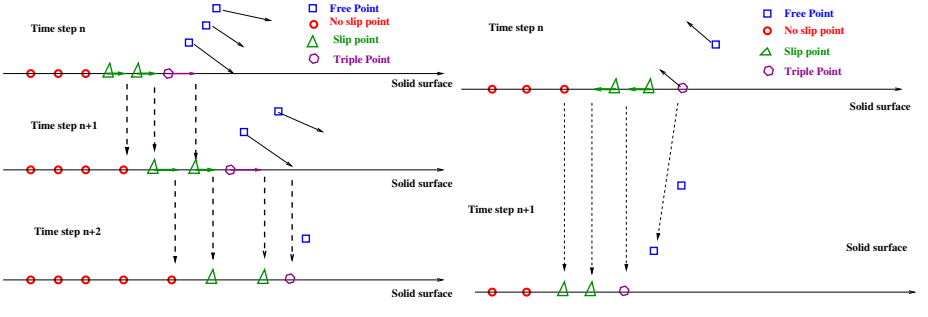

Fig. 1. *Left.* Circles represent no-slip nodes, triangles represent slip nodes $u_z = 0$, squares represent "free" nodes, diamond is the triple point. *Right.* Circles represent no-slip points $\boldsymbol{u} = 0$, triangles represent slip points $u_z = 0$, squares represent "free" points, diamond is the triple point.

4 Numerical Results

We consider a water droplet. The reference length and velocity are: $L_{ref} = 2.3\,mm$, $U_{ref} = 0.98\,m/s$. Then, $Re = \dfrac{\rho U_{ref} L_{ref}}{\mu} \approx 46$, Weber number $We = \dfrac{\rho U_{ref}^2 L_{ref}}{\sigma} \approx 68$ and $C_a = \dfrac{\sigma}{\mu U_{ref}} \approx 1.5$.

4.1 Spreading Phase Using a Tanner Type Law

We start by testing the efficiency of the algorithm. To this end, we consider the Tanner type law as triple line dynamic modelling, and we make fit this law with available experimental data, [1], related to a spreading phase. The triple point position is imposed at each time. We focus on the volume conservation, the height and diameter of the spreading (splat radius) and the deformation of the mesh (number of re-meshing necessary), see Fig. 2. With a time step $dt = 5.10^{-5}s$ and a coarse mesh (≈ 600 elements), volume lost after 650 iterations is roughly 3%. The loss occurs mainly at the very beginning of spreading. Mesh transport is efficient hence re-meshing occurs only when a projection occurs (see previous section). From a qualitative point of view, numerical results are similar to experimental data, [1].

4.2 Influence of the Local Parameters ($\boldsymbol{\beta, g, h}$)

We present some influence of terms specific to the Shikmurzaev's model by considering the following steady-state Stokes system: Find $(\boldsymbol{u}, p)$ such that:

$$\begin{cases} 2\displaystyle\int_\Omega D(\mathbf{u}) : D(\mathbf{v})dx - \int_\Omega p\, div(\mathbf{v})dx + 2\int_\Omega \mathbf{u}_a\mathbf{v}dx + \beta\int_{\Gamma_{slip}} u_r\, v_r\, ds \\ \qquad = \displaystyle\int_{\Gamma_{free}} \frac{\kappa}{Ca}\,\mathbf{v}\,\mathbf{n}ds + \int_{\Gamma_f} h\,\mathbf{v}\,\tau\, ds - \int_{\Gamma_{sl}} g_r\, v_r ds, \quad \forall \mathbf{v} \\ \displaystyle\int_\Omega div(\mathbf{u})\, q\, dx = 0, \quad \forall q \end{cases}$$

We fix one of the three parameters and we simulate the Stokes system with different values for the other two. The set of absolute values used for the parameters is $\{0, 1, 10^2, 10^4\}$ with signs taken as described previously. We expect that

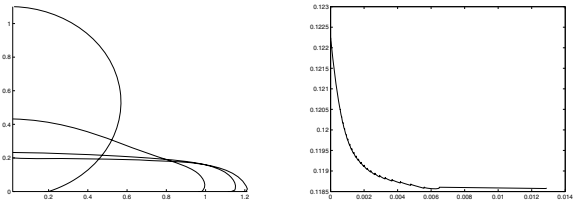

Fig. 2. Spreading: droplet profiles and volume in function of time steps

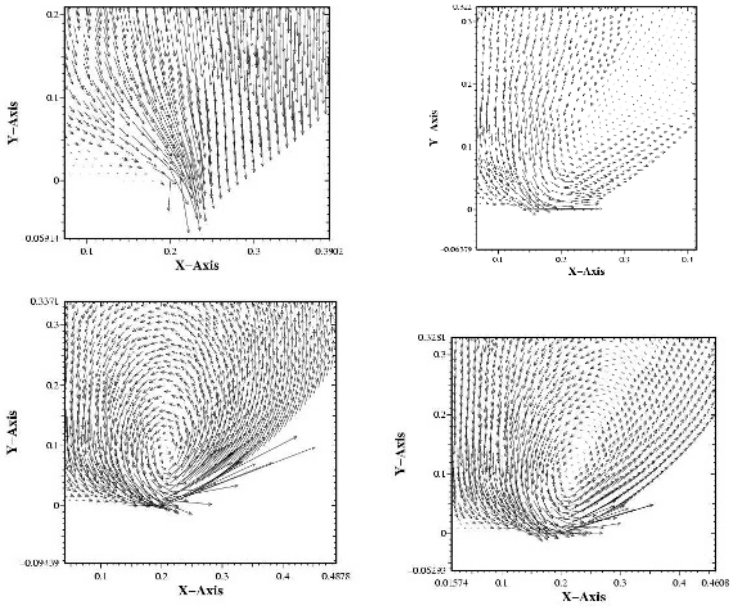

Fig. 3. Velocity in the vicinity of the triple point for $\beta = 10^2$ and $(g, h) = \{(0, 0), (-10^2, 0), (0, -10^2), (-10^2, -2 \times 10^2)\}$. Scale factors are $10, 0.5.0.1, 0.1$ respectively.

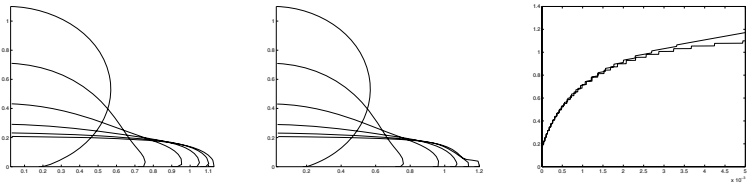

Fig. 4. Droplet profiles and triple point position (right) for $(\beta, g) = \{(10^3, -10), (10^3, -10^2)\}$

for a high β value, the effect of this term will be similar to a no-slip/slip boundary condition on Γ_{sl}. For the g-term, it is clear that a high $|g|$ will be equivalent to accelerating/decelarating the spreading. The h-term creates an upward force which should be responsible for recoiling, see Fig. 3, for $\beta = 100$ and different values of g and h.

4.3 Spreading Phase Using the Shikhmurzaev Model

We consider the spreading phase using the Shikhmurzaev's model and the algorithm presented previously. As mentioned above, g acts like a control on the position of the triple point. A decrease for $g < 0$ translates in a faster spreading. If g is small, this influence is likely not to be seen in the first part of the spreading, when the inertial forces dominate all other forces in presence. By increasing

Fig. 5. Droplet profiles for $(\beta, g, h) = \{(500, 100, 0), (100, 100, -10)\}$

$|g|$ over a threshold, which depends on β, it accelerates the spreading and modifies the flow nature. For $|g|$ large, large interface distortions occurs and mesh generator fails to re-mesh. In order to observe the influence of the g-term, we fix $\beta = 1000$, and we perform 1000 iterations with a step size of $dt = 5.0 \times 10^{-6}$ for $g \in \{-100, -10, -1\}$, Fig. 4. One can observe that after the inertial phase, the triple point position is farther to the right with a decreasing g.

4.4 Recoiling Phase Using the Shikhmurzaev Model

We consider the recoiling phase using the Shikhmurzaev model and the algorithm presented previously. Parameters are as follows: $(\beta, g, h) = (100, 100, -20)$ and $(500, 100, -20)$. As expected, the h-term controls the separation of the triple point from the solid surface, see Fig. 5, while the g-term helps the droplet to slide toward the symmetry axis. Combination of both lead to a recoiling motion. Let us precise that we observed the onset of free surface instabilities. A method to deal with these instabilities is under investigation.

5 Conclusion

We have discretized and implemented macroscopic part of the Shikhmurzaev model, [10], [2], using an ALE formulation and a finite element scheme. Also, a connection with Qian-Wang-Sheng's results, [11], is presented. The present model comprises generalized Navier slip boundary conditions with local surface tension gradient terms in the vicinity of the contact line. The local term values have been chosen upon a previous mathematical and numerical study done in [8]. To test the efficiency of the present algorithm, first we considered a classical mobility relation and we obtained spreading droplet profiles qualitatively comparable to experimental results. Then, we showed how the introduction of these new local terms in the vicinity of the contact line allow to model on one hand the spreading phase, on the other hand the recoiling phase. A full coupling between the macroscopic part and the microscopic part of the Shikhmurzaev model is under progress.

Acknowledgements. The authors would like to thank A. Soucemarianadin and JL. Achard from Laboratory of Geophysical and Industrial Fluid Flows -LEGI- Grenoble, France, for their numerous and fruitful discussions and remarks.

References

[1] Allaman S., Desie G., Vadillo D., Soucemarianadin A. : Impact and spreading of micro-drops onto solid substrates. Mcaniques & Industries **4** (2003) 443-455.

[2] Blake T.D., Bracke M., Shikhmurzaev Y.D. : Experimental evidence of nonlocal hydrodynamic influence on the dynamic contact angle. Physics of fluids **11** (1999) 1995-2007.

[3] de Gennes P.G.: Wettings: statics and dynamics. Reviews Modern Phys. **57** (1985) 827-863.

[4] Dussan V.E.B., Davis S.H. : On the motion of a fluid-fluid interface along a solid surface. J. Fluid Mech. **65** (1974) 71-95 .

[5] Hocking L.M. : A moving fluid interface. Part II. The removal of the force singularity by a slip flow. J. Fluid Mech. **79** (1977) 209-229 .

[6] Jacqmin D. : Contact-line dynamics of a diffuse fluid interface. J. Fluid. Mech., **402** (2000) 57-88.

[7] Monnier J. : Modélisation Numérique de la Ligne Triple. Internal Report LMC-IMAG, Summer school CEA Grenoble. September (2003).

[8] Monnier J., Witomski P. : Analysis of a Local Hydrodynamic Model with Marangoni Effect. J. Sc. Comp. **21** (2004) 369-403.

[9] Pomeau Y. : Recent progress in the moving contact line problem: a review. C.R. Mécanique. **330** (2002) 207-222.

[10] Shikhmurzaev Y.D. : The moving contact line problem on a smooth solid surface. Int. J. Multiphase Flow. **19** (1993) 589-610.

[11] Qian T., Wang X-P., Sheng P. : Generalized Navier boundary condition for the moving contact line. Comm. Math. Sci. **1** (2003) 333-341.